Journal of Solid State Chemistry 226 (2015) 170–178

Contents lists available at ScienceDirect

Journal of Solid State Chemistry

journal homepage: www.elsevier.com/locate/jssc

Supramolecular intermediates in the synthesis of polymeric carbon nitride from melamine cyanurate

Roberto C. Dante [a,*], Francisco M. Sánchez-Arévalo [b], Pedro Chamorro-Posada [c], José Vázquez-Cabo [d], Lazaro Huerta [b], Luis Lartundo-Rojas [e], Jaime Santoyo-Salazar [f], Omar Solorza-Feria [g]

[a] Facultad de Mecánica, Escuela Politécnica Nacional (EPN), Ladrón de Guevara E11-253, Quito, Ecuador
[b] Instituto de Investigaciones en Materiales, Universidad Nacional Autónoma de Mexico, Apdo. Postal 70-360, Cd. Universitaria, Mexico D.F. 04510, Mexico
[c] Dpto. de Teoría de la Señal y Comunicaciones e IT, Universidad de Valladolid, ETSI Telecomunicación, Paseo Belén 15, 47011 Valladolid, Spain
[d] Dpto. de Teoría de la Señal y Comunicaciones, Universidad de Vigo, ETSI Telecomunicación, Lagoas Marcosende s/n, Vigo, Spain
[e] Centro de Nanociencias y Micro y Nanotecnologías—IPN, Luis Enrique Erro s/n, U. Prof. Adolfo López Mateos, 07738 Ciudad de Mexico, Distrito Federal, Mexico
[f] Departamento de Física, Centro de Investigación y de Estudios Avanzados del Instituto Politécnico Nacional, CINVESTAV-IPN, Apdo. Postal 14-740, Mexico D.F. 07360, Mexico
[g] Departamento de Química, Centro de Investigación y de Estudios Avanzados del Instituto Politécnico Nacional (CINVESTAV), Av. IPN 2508, Col. San Pedro Zacatenco, Apdo. Postal 14-740, Mexico D.F. 07360, Mexico

ARTICLE INFO

Article history:
Received 8 December 2014
Received in revised form
27 January 2015
Accepted 24 February 2015
Available online 5 March 2015

Keywords:
Carbon nitride
Supramolecular intermediates
Nanosheets
THz spectroscopy
Solid solvents

ABSTRACT

The adduct of melamine and cyanuric acid (MCA) was used in past research to produce polymeric carbon nitride and precursors. The reaction yield was considerably incremented by the addition of sulfuric acid. The polymeric carbon nitride formation occurs around 450 °C at temperatures above the sublimation of the adduct components, which occurs around 400 °C. In this report the effect of sulfuric acid on MCA was investigated. It was found that the MCA rosette supramolecular channel structures behave as a solid solvent able to host small molecules, such as sulfuric acid, inside these channels and interact with them. Therefore, the sulfuric acid effect was found to be close to that of a solute that causes a temperature increment of the "solvent sublimation" enough to allowing the formation of polymeric carbon nitride to occur. Sulfate ions are presumably hosted in the rosette channels of MCA as shown by simulations.

© 2015 Elsevier Inc. All rights reserved.

1. Introduction

Polymeric carbon nitride, apart from its applications as the precursor for the synthesis of superhard carbon nitride phases [1–10], has also been investigated for a number of other applications [11–15]. For example, combining the chemical sensitivity with the optical and semiconductor properties, polymeric carbon nitride has become an interesting candidate into the wide field of sensors [16–20].

The pathway synthesis presented by Li et al. [21] was extended to heteroatoms different from halogens by Dante et al. [22–25]. In the last developments, the polycondensation reaction (see Eq. (1)) was carried out starting directly from melamine cyanurate – the adduct of melamine and cyanuric acid – which crystallizes in layers like graphite [16].

$$C_3N_3(NH_2)_3 \cdot C_3N_3(OH)_3 \rightarrow C_6N_7(NH)(NH_2) + 3H_2O \quad (1)$$

This reaction is promoted by sulfuric acid, which acts as a catalyst [22–25]. The results of the melamine cyanurate pyrolyzed in the range between 450 and 700 °C were presented in previous reports [24–26], with the significant result being the formation of crumpled and globular particles of polymeric carbon nitride with thickness ranged between 5 and 25 nm.

On the contrary, the intermediates obtained with this reaction are almost unexplored and represent a new class of carbon nitrogen materials. The choice of this reaction pathway was based on the work of Heine et al., who reported the formation of melaminium sulfate [23] which is more stable than melamine cyanurate by itself, which sublimates around 430 °C preventing the condensation reaction into the heptazine unit-based polymer called polymeric carbon nitride. Heine et al. reported the supramolecular 3D assembly of $[(LH)_2(SO_4)_2]_n$ [23].

In the case of melamine cyanurate (melamine-cyanuric acid adduct, MCA), the intermediates are more complex than the final products and similar to that reported by Heine et al. They are bound mainly through hydrogen bond, π–π interactions, and interaction between ions making them a supramolecular assembly. Their UV–vis absorptions and structure are different from both

* Corresponding author.
E-mail address: rcdante@yahoo.com (R.C. Dante).

http://dx.doi.org/10.1016/j.jssc.2015.02.018
0022-4596/© 2015 Elsevier Inc. All rights reserved.

the final product and the reagents. However, they seem to be organized in layers which then eventually evolve to the polymeric carbon nitride structure after thermal treatment at temperatures above 450 °C [23].

The interest on anion directed self-assembly processes have increased notoriously due to their use in the development of novel nanosized materials. In contrast to the metal containing coordination polymers, where coordination bonds dominate, anion based networks are stabilized by multiple weak interactions such as hydrogen bonding or electrostatic and π-interactions; nevertheless, the skillful use of these forces may result in functional molecular units with interesting properties. In fact, this may result in materials with a different sensitivity to the surrounding environment, due to their weak interactions that assembled the structure, opening to a new class of sensors for anions [27]. In our materials, the presence of sulfur belonging to sulfate ion is low; as it was shown in our previous work [25]; in the present one, is not far from 2% on atomic base leading to a significant content of sulfate ions. Simulations reported by Whitesides et al. [28] showed that the linear tape motif of the arrangement of 1:1 MCA adduct may likely be modified by substituents which a steric hindrance leads to either a crinkled or rosette arrangements [28]. That is an example of a case of non-covalent synthesis. In fact, Ranganathan et al. [29] detected that the actual arrangement obtained under hydrothermal synthesis of MCA was the hexamer rosette one (see Fig. 1), which is held together by hydrogen bonds by the type: N–H–H, and N–H–O with a small channel of 4 Å diameter resembling cryptands. Moreover, a similar arrangement was found for the tritiocyanuric acid and melamine. This situation, together with the sulfur content means that there is approximately a sulfate ion per each rosette hexamer [29].

TeraHertz-time domain spectroscopy (THz-TDS) was used to confirm the presence of a stacked and turbostractic structure of the intermediates to find some correspondence with the final product that was already studied by this spectroscopy technique that can reveal lattice vibration modes; in fact this technique was able to reveal a vibration mode of the sheets along the stacking direction [26]. In THz-TDS, the terahertz signal is generated by the conversion to base-band of a train of ultrafast optical pulses generated with a femtosecond laser. This is typically performed using either semiconductor photoconductive antennas or optical rectification in a nonlinear medium. The pulses are then propagated into (or reflected from) the medium under test and their short duration ensures that their spectra cover the terahertz spectral region of interest. The received terahertz signal can be detected with a gated photoconductive antenna where a delayed version of the optical pulses is used as the control signal. The analysis of the obtained terahertz waveforms with or without test sample permits to determine material parameters. The unexpected result of this study was to find that MCA may act as a solid supramolecular solvent able to host small molecules inside the rosette-shaped channels and interact with them, as in the case of sulfuric acid. Moreover, it seems that the structure is only slightly altered. However, this solution-like behavior causes a significant increment of the sublimation temperature of the MCA components thus allowing solid MCA to reach a temperature high enough to react and form heptazine polymers.

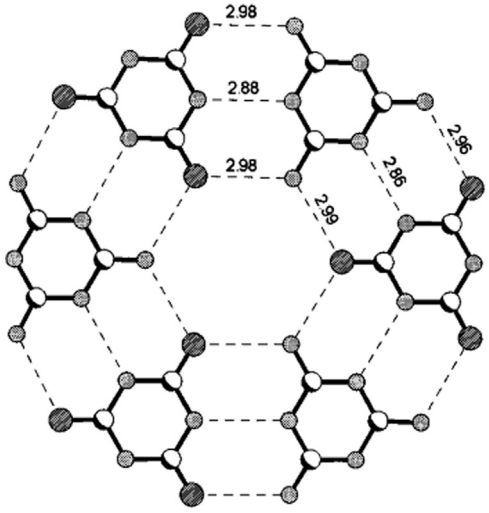

Fig. 1. The rosette formed between cyanuric acid and melamine. Dashed lines represent hydrogen bonds. Adapted with permission from [29], Copyright 1999 American Chemical Society.

2. Materials, experimental and theoretical methods

2.1. Materials

The reagent, melamine cyanurate was supplied by Quartz S.r.l. (Italy) with a purity higher than 99%. Melamine cyanurate was manually milled in an agate mortar for about 5 min; subsequently the sample was treated with 1 M sulfuric acid overnight and dried at 110 °C for 6 h. The sulfuric acid-treated samples, each one of about 4 g, were placed in a ceramic crucible and thermally treated at different temperatures between 250 and 400 °C in air in a convective oven for 30 min at the maximum temperature. The three samples obtained were denominated CN1 (250 °C), CN2 (300 °C), and CN3 (400 °C). It was found that sulfuric acid acts as a catalyst as described in more detail in our previous report [25].

2.2. Structural characterization

2.2.1. X-ray diffraction measurements

The X-ray diffraction patterns were obtained by means of a powder diffractometer Rigaku ULTIMA-IV with Cu *Kα* radiation. Glass capillaries for sample mounting were used. The samples were ground in an agate mortar and sifted. The measurements always lasted for 1 h, and crystalline silicon was used as a standard.

2.2.2. FT-IR spectroscopy

The infrared spectra were obtained by means of a Thermo Nicolet 380 Fourier transform-infrared (FT-IR) sepectrometer (Nicolet, USA). KBr tablets of the specimens were used to identify the chemical functional groups.

2.2.3. TEM and SEM characterization

Transmission electron microscopy (TEM) was performed with a JEOL JEM-FS2200 HRP (JEOL, Japan) and scanning electron microscopy by a JEOL JSM-820 SEM with energy-dispersive X-ray spectroscopy (EDS) probe (JEOL, Japan).

2.2.4. Thermal analysis

The thermal stability and decomposition rate of supamolecular intermediates in of polymeric carbon nitride from melamine cyanurate was evaluated by thermogravimetric analysis using a STD Q600 thermobalance (TA Instruments) with an nitrogen mass flow rate of 25 mL/min and a temperature raye of 10 °C/min.

2.2.5. UV–vis spectroscopy

UV–vis diffuse reflectance spectra were measured using a Perkin Elmer Lambda 35 UV–vis spectrophotometer. A Spectralon® blank was used as reference. The reflectance data were transformed to absorbance data applying the Kubelka–Munk method as follows:

$$F(R) = \frac{(1-R)^2}{2R} \quad (2)$$

where R is the reflectance and $F(R)$ is the Kubelka–Munk (K–M)

function. The K–M function was plotted as a function of the energy ($E=hc/\lambda$) and the band gap value was calculated through the inflection point of this curve. The abscissa of this point is directly associated with the band-gap value [30].

2.3. TeraHertz-time domain spectroscopy measurements

A Menlo Tera K15 Spectrometer was used for the THz-TDS analysis. The system is based on a 1560 nm fiber laser that generates 90 fs pulses at a repetition rate of 100 MHz. This provides a compact fiber-coupled setup. The system was operated in a nitrogen rich atmosphere in order to avoid the signature of water absorption in the recorded samples. Ten sample and ten references measurements were performed in each case in order to reduce the noise in the measurements.

The material parameters in the spectral range of interest were calculated from the time domain photocurrent traces measured with the spectrometer. These time domain waveforms depend not only on the material data but also on the width of the pellets due to the contributions from multiple reflections at the pellet–air interfaces. Signal processing techniques similar to those described by Duvillaret et al. [31] were employed in order to obtain the THz spectra of the materials.

2.4. X-ray photoelectron spectroscopy

X-ray photoelectron spectroscopy was carried out by means of a K-Alpha model spectrometer by Thermo Scientific making use of a monochromatic source of Al*K*α (1487 eV). The vacuum pressure of the analysis cage was 10^{-9} mBar during the whole experiments and there was used a spot size of 400 μm. The spectra of high resolution (narrow sacans) were obtained using a pass energy of 60 eV.

2.5. Quantum chemistry computations

The semiempirical quantum chemistry computations were performed with the PM6 method [Stewart2007] using the parallel implementation for multi-threaded shared-memory CPUs and massively parallel GPU acceleration [32] of the MOPAC2012 [33] software package. A Fedora Linux server with a 12 cores Intel Xeon processor and a NVIDIA Tesla K20 GPU was used for the computations.

3. Results and discussion

3.1. Infrared spectroscopy

The precursor melamine cyanurate is an adduct of melamine and cyanuric acid and exhibits a strong broad absorption between 2700 and 2500 cm^{-1} (not to be confused with the twin bands of gaseous CO_2 which are much narrower and less intense, located below 2400 cm^{-1}. It is noteworthy to point out the background was subtracted from all spectra). This is due to hydrogen bond as shown by its IR spectrum in Fig. 2. This band disappeared after treatment with sulfuric acid; in addition, the two peaks due to N–H stretching between 3400 and 3200 cm^{-1} and the corresponding peak to N–H bending of primary amines at 1662 cm^{-1} were considerably decreased. This indicates a strong interaction between melamine and sulfate ions, as it was previously reported by Heine et al. [23].

After thermal treatments for CN1, CN2 and CN3, the band due to hydrogen bond was partially restored because of the sulfuric acid removal. However, significant changes occurred in the other parts of the spectrum. New bands appeared which can be associated to the heptazine ring formation; it was especially evident in CN3. The infrared spectroscopy shows that CN1 and CN2 are very close as inferred from the absorption bands shown in Fig. 3. The interpretation of the bands is quite difficult since there are several components' contributions: cyanuric acid, melamine and sulfuric acid (sulfate ion). In the spectrum of CN1 some characteristics belonging to both cyanuric acid and melamine were found. The three carbonylic bands between 1780 and 1700 cm^{-1} of cyanuric acid decreased and finally disappeared in the CN3 spectrum, as well as the C–O stretching bands between 1100 and 1000 cm^{-1}, and the wagging of primary amines at 760 cm^{-1}; this indicates that condensation occurred. Moreover, carbonyls and hydroxyls groups of cyanuric acid seemed to be involved into a strong hydrogen polymeric bonding as testified by the broad band between 2800 and 2000 cm^{-1} in CN1 and CN2 which definitely disappeared in CN3. This was a restoration to the original sample impregnated by sulfuric acid, where the adduct hydrogen bonds were disrupted. In the same way, the intense peaks between 1650 and 1527 cm^{-1}, corresponding to the mode of asymmetric and symmetric scissoring of primary amines, tended to decrease and revealed two weaker bands between 1610 and 1537 cm^{-1} (linked to vibrational modes belonging to melem ring [32]) in CN3, as well as the bands between 3400 and 3200 cm^{-1} of both asymmetric and symmetric NH stretching of primary amines considerably decreased. All the C–N stretching bands between 1430 and 1394 cm^{-1} associable to primary amines (linked to aromatic rings such as triazine) substantially decreased in CN3, while the secondary amine C–N stretching are much higher in the region between 1300 and 1100 cm^{-1} in comparison of both CN1 and CN2. In CN3 further condensation occurred forming more amine bridges and consequently more secondary amines, as shown by the increasing of the shoulders between 1274

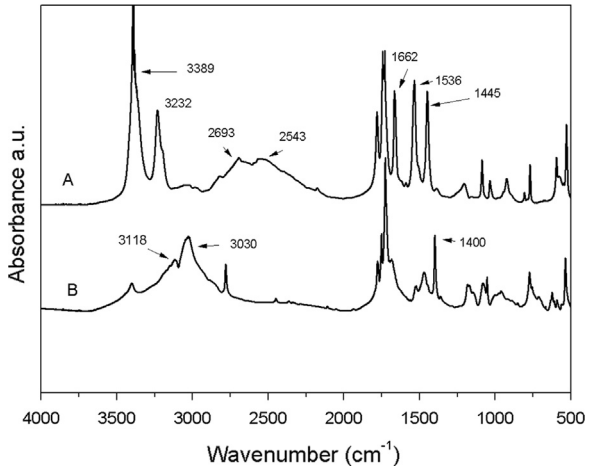

Fig. 2. IR spectra: (A) melamine cyanurate, (B) melamine cyanurate treated with sulfuric acid.

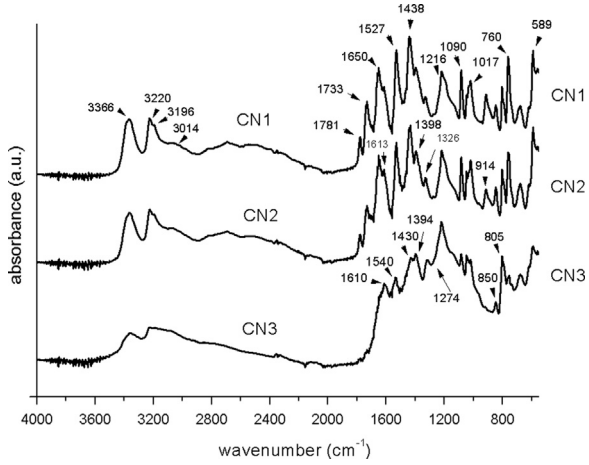

Fig. 3. IR spectra of CN1, CN2, and CN3 samples.

and 1240 cm^{-1} which probably belong to secondary or even tertiary amine bridges. The weak peaks at 805 and 850 cm^{-1}, which correspond to ring deformation modes, are more evident in CN3 with a considerable decreasing of the peak at 850 cm^{-1}. The latter band can be attributed to an E' ring deformation mode of a free heptazine unit with symmetry D_{3h}, while that at 805 cm^{-1} to a A_1 ring deformation mode of either dimers or e short polymers with symmetry C_{2v}. The bands around 1000 and 600 cm^{-1}, well defined for CN1 and CN2, can be attributed to sulfate S=O stretching and deformation, respectively. The main bands of CN3 are compatible with a tri-s-triazine or an intermediate stage. All the cyanuric acid bands probably disappeared due to condensation of rings and polymerization. The low definition of the bands is an indication that the material is highly amorphous in the stacking direction. Finally, the CN3 spectrum shows that, although the polymer formation advanced, there are consistent residues of the adduct.

3.2. Thermal gravimetric analysis (TGA)

The TGA curves, displayed in Fig. 4, show a different behavior for the three samples. Three onsets can be clearly distinguished in CN1 and CN2. The first one corresponds to almost inaltered melamine cyanurate which considerably loses mass from 350 °C. However, the other onsets can be attributed to two different species already present in the treated sample and not only formed during TGA execution, as can be inferred by the TGA of pure MCA, which showed the first onset around 400 °C corresponding to the MCA decomposition into gaseous melamine and cyanuric acid [25]. The second decomposition of MCA sample above 500 °C is due to the polymeric carbon nitride formed during the thermal gravimetric analysis. In CN1, CN2, and CN3 samples treated with sulfuric acid, the species that decomposed between 400 and 500 °C, according to the IR spectra and the structural simulation, can be mainly conformed by MCA interacting with sulfuric acid, while the last species which decomposed between 500 and 700 °C are possibly already polymerized heptazine rings (i.e. polymeric carbon nitride). In CN3 the latter is the most abundant species, while the reagent MCA is almost disappeared passing from the 50% present in CN1 to the 5% of CN3. It is noteworthy to point out that the intermediate species (MCA•H_2SO_4) is almost in the same amount as in CN1 and CN2 around the 20%, indicating that this is the intermediate which mainly converts and polymerizes into polymeric carbon nitride. The yield of the sulfuric acid treated samples is considerably more than that of the pure MCA.

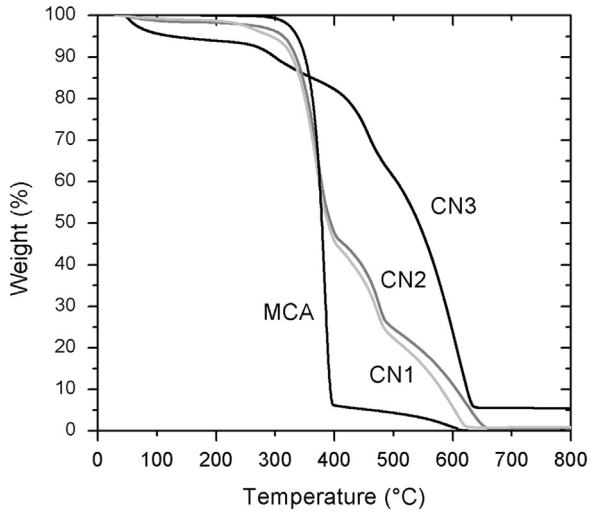

Fig. 4. TGA curves of the CN1, CN2, and CN3 samples from left to right.

The supposed reaction mechanism can be the following divided into two different pathways with different yield:

$$MCA \rightarrow CN_X \quad (3)$$

$$MCA \cdot H_2SO_4 \rightarrow CN_X \quad (4)$$

where MCA is the melamine cyanurate adduct, MCA · H_2SO_4 represents the MCA which is interacting with sulfuric acid, while CN_x stays for polymeric carbon nitride, x can vary depending of the degree of polymerization (hydrogen atoms in this case has been neglected for brevity only, in any case their number in the formula depends also on x). The pathway of Eq. (3) corresponds to the MCA which is not interacting with sulfuric acid and its yield is very low (around of 5% reacted) as can been inferred by the TGA curve of MCA alone. It is reasonable that till the MCA is not completely consumed the intermediate MCA · H_2SO_4 content will remain quite constant.

3.3. Estimation of the band-gap

Fig. 5 shows the UV–vis spectra, where $F(R)$, as a function of photon energy, is shown for supramolecular intermediates in of polymeric carbon nitride from melamine cyanurate. The band gap values were estimated using the K–M absorbance function and they are summarized in Table 1. Note that this gap-band values correspond to a semiconductor n-type polymer network, according to previous reports [25].

It is noteworthy to point out that the absorption around 4.5–3.0 eV grew up passing from CN1 to CN3, which is probably a phenomenon linked to the heptazine ring formation. However, the weak broad absorption around 2.5 eV (underlined in Fig. 5 with a dashed line only for CN1), possibly linked to formation of transient cations like melaminium, disappeared in CN3. Combining these observations with the IR detection of adduct residues in CN3, we can conclude that all the specimens are a blend of reagents, intermediates and products. The latters increased their content passing from CN1 to CN3 overwhelming intermediates and reagents.

3.4. X-ray photoelectron spectroscopy results

The XPS surveys of the samples show the presence of C1s, N1s, O1s (belonging to both intermediates and sulfate ions), S2p and S2s peaks (see Fig. 6). XPS results of CN1, CN2 and CN3 show the presence of the following bonds: C–N, C=N, –OH, and C–NH

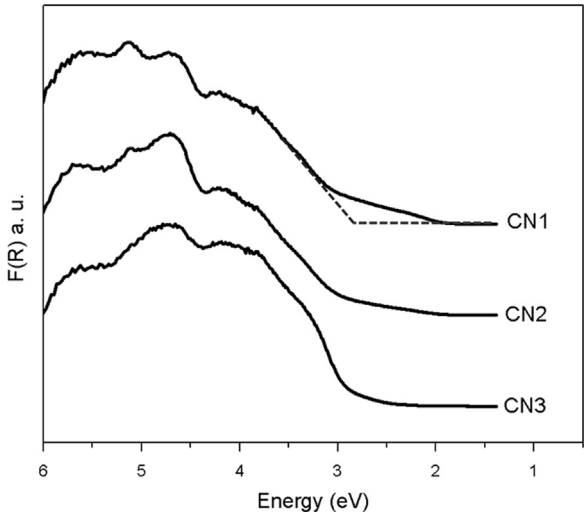

Fig. 5. UV–vis spectra of CN1, CN2, and CN3 samples. The weak absorption around 2.5 eV is underlined with a dashed line for CN1.

compatible with the lactim form of cyanuric acid. Moreover, it is possible to observe the formation of tri-s-triazine rings and other residues, principally C–C, C–CH, C–CH_2 and C–O–N.

Table 2 shows the binding energies corresponding to the C1s and N1s due to the specific bonds present in the samples. The basic model of chemical structure of the polymer is shown in Fig. 7 , in order to favor the identification of the bonding and atom types. This model was reported by R.C. Dante et al. [25], where each atom is numbered, and the assignment carried out by XPS follows this labeling system for heptazine units.

The C1s and N1s spectrum for the samples and their corresponding deconvolution curves are shown in Fig. 8. The peak C1s core level of CN1 content contributions of 284.80 eV binding energy corresponds to the C–C bonds of the graphitic carbon, and the peaks at 285.70, 286.27, 287.14, 288.25, 288.79, 289.80, and 290.68 eV can be attributed to C–CH, CH_2, C–N, C=N, C–O, C=O and C–O–N bonding, respectively. Initially, CN1 contained large amounts of functional groups, but after the annealing treatment, a substantial loss of functional groups was observed for both CN2 and CN3, as shown in Fig. 8.

The contribution of C–O–N and C=O in CN2 and CN3 is much lower than that of CN1. The C–O–N and C–O peaks considerably decreased and C=O finally disappeared. The C=N and C=O bonds are present in all the samples so that is probably due to the presence of lactam forms. In the CN1 sample it is possible to see that all the carbon bonds are of intemediates. However, the carbon atoms named C1 and C2 (see Fig. 8 and Table 2) with binding energy of 288.15 and 288.58 eV, respectively, which belong to the heptazine ring, were already present in CN1 with proportion 1:1.

Looking at C 1s in Fig. 8, the presence of C–O–N is detected at 290.68 eV, which disappeared in CN3. Another noticeable aspect is the disappearance of C–N band at 288.79 eV. On the other hand, it is possible to see that heptazine rings were formed in CN2 and CN3 with an increment ratio of 1: 1.6. The same proportion is fulfilled for the satellite shake up C1s corresponding to the delocalized electrons de $\pi \rightarrow \pi*$ transition.

In N 1s there are six contributions found in deconvolution curves. Here, the main peaks can be identified as N1 (nitrogen of the ring i.e. C–N=C), N2 (a secondary amine i.e. C–N–H), and N3 (primary amine) (see Fig. 8 and Table 2)) at 398.86 eV, 400.30 eV and 401.07 eV, respectively. The other three peaks are C–O–N at

Table 1
Shows the optical band-gap values for CN1, CN2 and CN3.

Sample	E_g(eV)
CN1	2.792
CN2	2.879
CN3	2.845

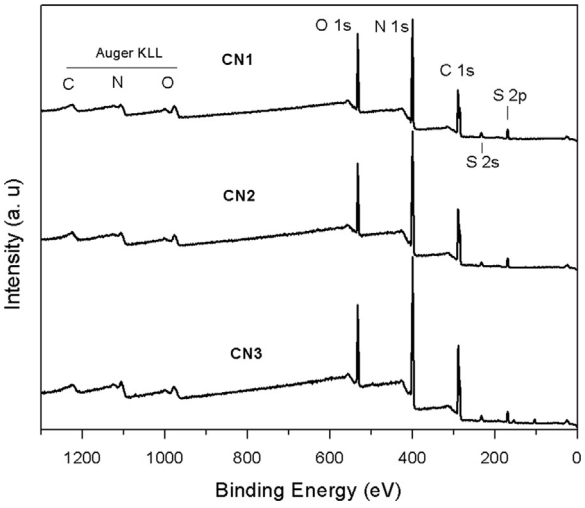

Fig. 6. Survey XPS spectra of intermediate polymeric carbon nitride from melamine cyanurate of the three annealed samples CN1, CN2, and CN3.

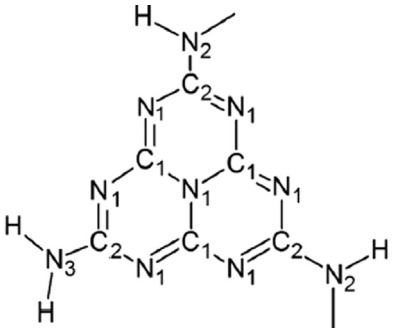

Fig. 7. Structure of heptazine ring (polymeric carbon nitride unit) according to XPS assignations.

Table 2
Binding energies corresponding to the C 1s and N 1s due to the specific bonds present in the samples.

C 1 s										
Sample	**C1**	**C2**	**C–CH_2**	**C–C**	**Cπ**	**C–N**	**C=N**	**C–O**	**C=O**	**C–O–N**
Binding energy (eV)[a]										
	288.15	288.58	286.27	284.8	193.91	287.14	288.25	288.79	289.80	290.65
Content (%)[b]										
CN1	0	0	3.5	28.4	0	1.6	18.9	18.5	19.8	5.4
CN2	7.3	7.3	2.6	28.2	1.1	3.8	13.8	16.0	13.6	2.6
CN3	12.1	12.0	4.7	28.2	1.8	1.5	31.7	0	8.2	0

N 1s						
Binding energy (eV)						
	N1	**N2**	**N3**	C–O–N	**C=N**	**Nπ**
	398.86	400.30	401.07	401.30	399.85	405.11
Content (%)						
CN1	33.3	11.3	20.2	3.0	31.4	0
CN2	42.9	17.7	13.3	2.4	21.9	1.8
CN3	55.3	15.6	12.4	0	12.9	3.9

[a] The uncertainity of the binding energy were estimated in ±0.05 eV.
[b] The chemical concentration percent of relative uncertainity is ±5%.

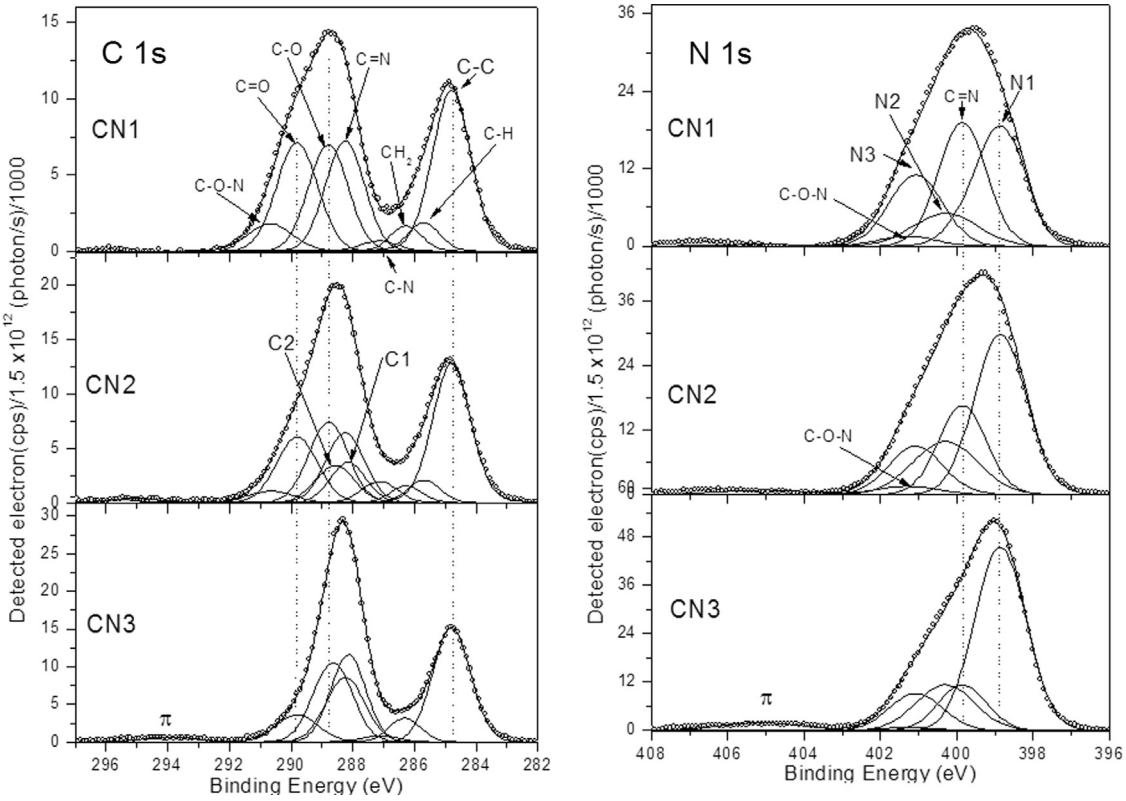

Fig. 8. The XPS deconvolution spectrum of C 1s and N 1s of the CN1, CN2, and CN3 samples.

401.30 eV, C=N at 399.85 eV and the satellite shake up of N π→ π* localized at 405.11 eV.

Calculations from the areas of the peaks showed that the sulfur contents based on the S 2p peak were 1.74, 2.37, and 2.35 atomic % for CN1, CN2, and CN3, respectively.

While the nitrogen atomic % were 43.18, 41.64, and 42.53, respectively.

These values correspond approximately to a sulfate ion per two rosette hexamers (Fig. 1) so that Eq. (4) can be rewritten in the following way:

$$[C_3N_3(NH_2)_3 \cdot C_3N_3(OH)_3]_3 \cdot H_2SO_4 \rightarrow$$

$$\rightarrow (NH_2)_2[C_6N_7NH_2(NH_x)]_{1+x} \cdot H_2SO_4 \rightarrow (NH_2)_2[C_6N_7NH_2(NH_{n-1})]_n \quad (5)$$

where x may take the values 0 and 1, while $n \geq 2$. Since the presence of OH was detected by IR and XPS, we can infer that some cyanuric acid molecules, as well as some melamine ones, may be protonated. Sulfate ions are present in the channels to stabilize these charges, and possibly stabilize also the MCA structure displacing the decomposition to higher temperatures allowing the heptazine formation.

In summary, MCA acts as a solid supramolecular solvent whose basic molecules are linked by weak but diffuse forces, as in other polar solvents, but with the difference that in MCA order is more extended. In this case solute molecules stay in the channels formed by the typical rosette arrangement.

We can say for analogy that the phenomenon we observe in the late decomposition at temperatures that allows the formation of heptazine (above 400 °C) is due to the same phenomenon that makes increase the boiling point in liquid solutions, i.e. the attraction forces between solvent and solute. In fact, the decomposition here is really the sublimation (like boiling for a liquid solution) of the gaseous cyanuric acid and melamine rather than a true solid decomposition of pyrolyzed products.

3.5. X-ray diffraction results

The XRD patterns of CN1, CN2 show a material with low crystallinity and peaks characteristic of MCA but with peaks that are clearly doubled, i.e. the pair at 10.80° and 11.76° as well as those at 27.31° and 27.97° (see Fig. 9). The intensity of these peaks decreased from CN1 and CN2, while in CN3 are very low and only a very wide broad band around 23° is visible, which may belong to amorphous sp^2 carbon in accordance with XPS spectra. No signal of ordered heptazine or polymeric carbon nitride is detected, the samples seem to be quite amorphous, especially CN3 which is mostly composed of heptazine compounds.

The XRD patterns seem to be not altered by the presence of the sulfate which is present in a considerable amount in all the samples as detected by XPS. However, in the case of the rosette arrangement, the channels of 4 Å are large enough to host the sulfate ions, approximately one for each rosette hexamer without considerably altering the material structure (distortions are possible for the hydrogen bonds). The disgragation of the MCA framework and the consequent disappearence of the channels prevented the formation of an ordered structure in CN3 mostly composed of heptazine compounds, which apparently have not a channeled structure as MCA [26].

Also morphology of particles changed during the process from CN1 to CN3. The platelet particles, shown in the SEM pictures of Fig. 10, which are almost similar in CN1 and CN2 with diameter around 1 μm, were replaced by much more fragmented particles with size sometimes below 1 μm, although the platelet structure was still present. Moreover, a TEM image reveals a nanoflake crumpled structure, which was extensively discussed in a previous report [25].

3.6. Quantum chemistry semiempirical calculations

The melamine cyanurate geometry was optimized using the PM6 method implemented in MOPAC assuming periodic boundary

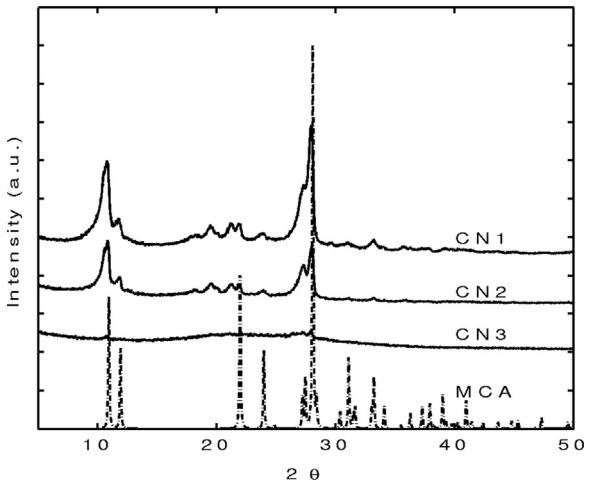

Fig. 9. XRD patterns of CN1, CN2, and CN3, and comparison with the simulated XRD.

conditions. Alternating layers with the positions of cyanurate and melamine interchanged between layers was assumed. The lattice parameters obtained are $a=14.882$ Å, $b=9.920$ Å, $c=7.364$ Å, $\alpha=90.55^\circ$, $\beta=94.03^\circ$ and $\gamma=90.29^\circ$. This is in very good agreement with the actual crystal parameters of MCA [29]: $a=14.853$ Å, $b=9.641$ Å, $2c=7.1620$ Å, $\alpha=90^\circ$, $\beta=92.26^\circ$ and $\gamma=90^\circ$. The geometry is displayed in Fig. 11, where the computational volume spanning $1\times1\times2$ unit cells has been outlined. Using for the computations two cells of the geometry with alternating layers in the c direction permits to meet the MOPAC requirement of a computational unit cell large enough to hold a sphere with a diameter of 8 Å [32–35].

Fig. 12 shows, in the top curve, the predicted powder XRD corresponding to the optimized molecular model calculated using MERCURY [36] software package and in the bottom curve the predicted pattern obtained from the structure published in the seminal work by Rao et al. [29]. The agreement between the two results is very good and there is also a very good correspondence with the measured data for both CN1 and CN2 (see Fig. 10). The

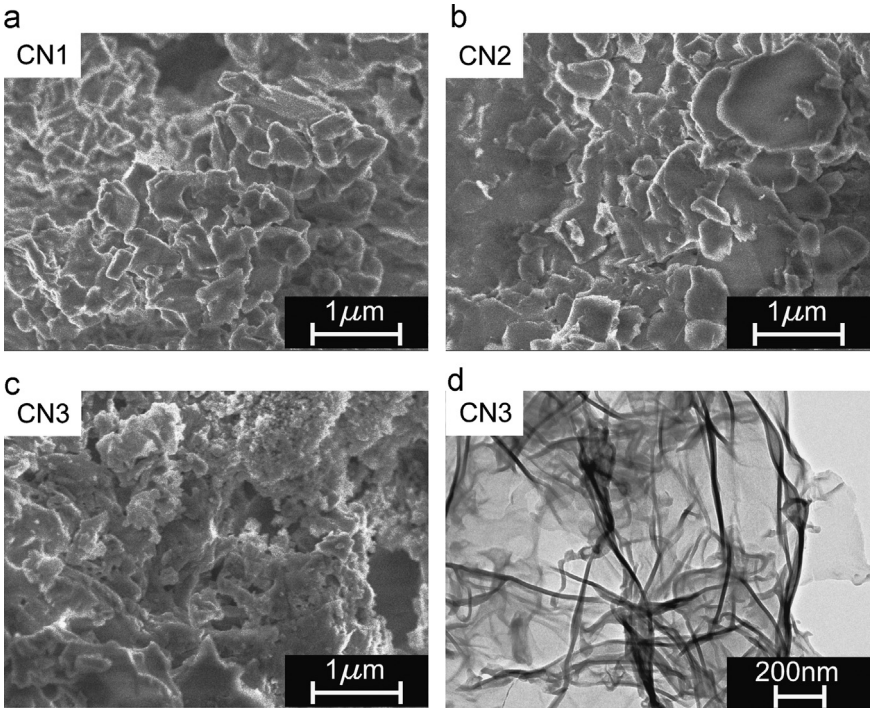

Fig. 10. SEM images of CN1 (a), CN2 (b), and CN3 (c). TEM image of CN3 (d).

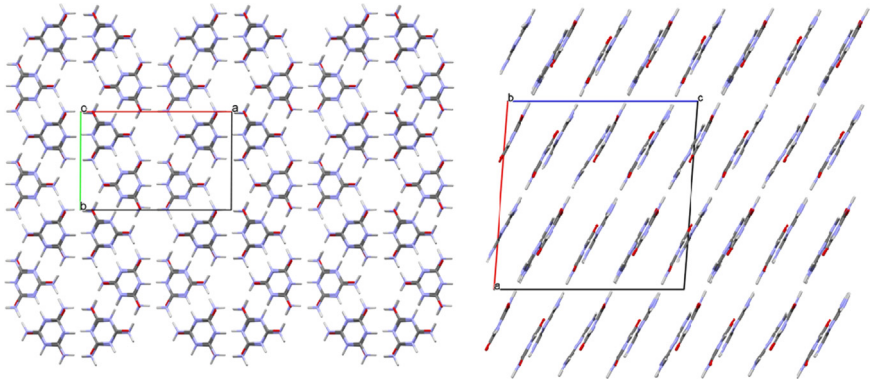

Fig. 11. Views of the PM6 MCA optimized geometry along the b and c axis. The computational domain spanning $1\times1\times2$ unit cells is outlined.

differences found in the measurements for these two samples can be attributed to a varying concentration of MCA in the samples.

The Fig. 13 displays the geometry of MCA incorporating the H_2SO_4 molecules in the rosette channels optimized using the PM6 Hamiltonian [37]. Even at this very high concentration, with every other channel fully saturated, the distortion of the MCA geometry is very small, with lattice parameters $a=14.958$ Å, $b=10.280$ Å, $c=7.961$ Å, $\alpha=89.75^\circ$, $\beta=94.80^\circ$ and $\gamma=89.94^\circ$. This illustrates the power of MCA for incorporating the H_2SO_4. At smaller concentration levels, as observed in the samples, with sulfuric acid scattered at random in the MCA host, a negligible effect on the main features of the XRD measurements is expected.

The vibrational spectrum in the THz band associated to the molecular model displayed in Fig. 11 was studied using MOPAC with the PM6 Hamiltonian [37]. This analysis confirms that the geometry corresponds to a true ground state. Fig. 14 shows an estimate of the normalized THz absorption curves in the band between 1.1 THz and 2.3 THz obtained from the calculated vibrational frequencies and the associated intensities assuming a Lorentzian lineshape with a linewidth of 3 cm^{-1} using Gabedit [38]. As opposed to other related materials [26] a large number of vibrational modes is found along this band.

3.7. THz-TDS spectroscopy measurements

Fig. 15 shows the measured attenuation spectra in the THz band. The results for CN1 and CN2 display similar features. In particular, the two bands obtained by the theoretical calculations performed for MCA can be identified, even though the main absorption peak appears shifted to higher frequencies in the calculations. The agreement between theory and experiment on this regard is within the expected accuracy limits of the semi-empirical calculations. Nevertheless, other factors can also be responsible of this shift, such as the existence of a relatively large number of vibrational modes contributing to the attenuation band and how the sulfuric acid present in the rosette channels can affect in different manners to the various resonances. The main difference between the CN1 and CN2 spectra is the reduction of the maximum absorption of the main peak in the spectrum of CN2 when compared with that of CN1. This could be the result of a decrease of the MCA relative presence in the CN2 sample. For CN3, the shape of the attenuation spectrum is completely different and the peak observed close to 2 THz can be linked to the dominance of the polymeric CN_x in the sample [26]. In relation with these results, we highlight the very high sensitivity of THz-TDS spectroscopy to morphological changes in the material under study, as it was previously found in [26].

4. Conclusions

The real intermediate to the formation of polymeric carbon nitride is what can be defined a solution within a certain latitude. The solvent is the adduct melamine cyanurate (MCA), a supramolecular solid held together by hydrogen bonds, which provides rosette-shaped channels

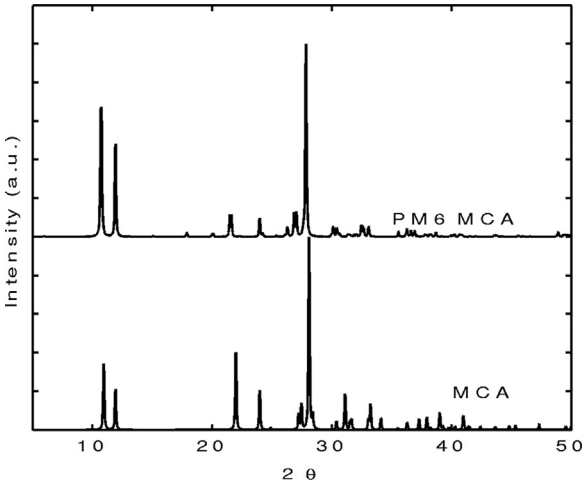

Fig. 12. Calculated XRD from the MCA PM6 optimized geometry.

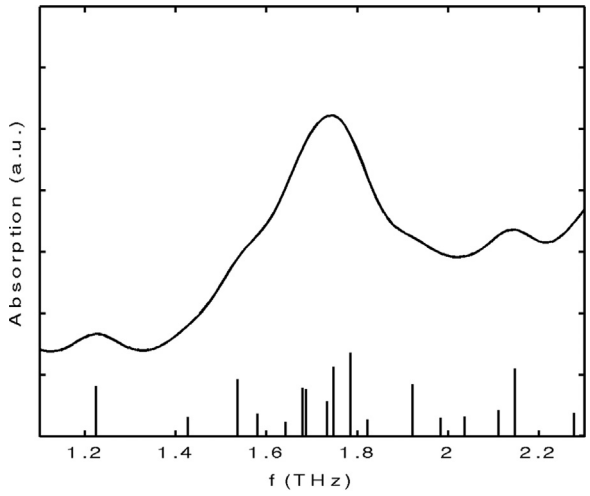

Fig. 14. Theoretically predicted normalized absorption spectra for MCA.

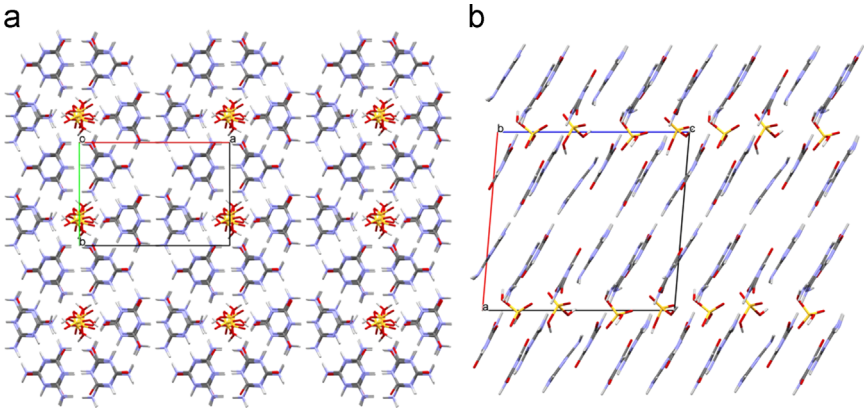

Fig. 13. Views along the *b* and *c* axis (panels (a) and (b), respectively), of the geometry for MCA incorporating H_2SO_4 optimized using the PM6 method. The computational domain spanning $1\times1\times2$ unit cells is outlined.

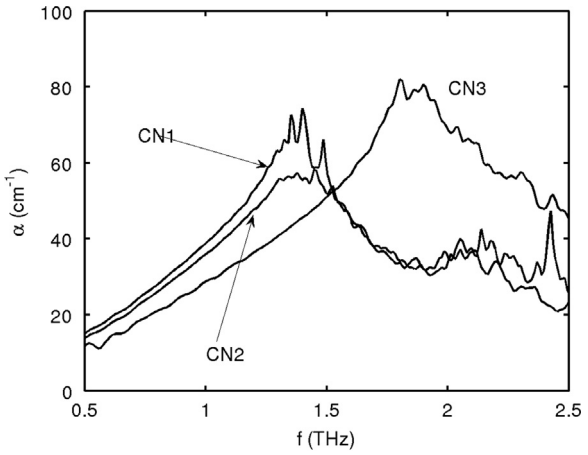

Fig. 15. Measured attenuation THz spectra.

with the possibility to host polar and ionic small molecules, as sulfuric acid, interacting with the wall "solvent" molecules. This "solution" exhibits a sublimation temperature higher than that of the pure "solvent" allowing the solvent molecules (cyanuric acid and melamine) to react to form heptazine and ultimately polymeric carbon nitride with a considerable yield increment with respect the pure melamine cyanurate. It is noteworthy to point out that melamine cyanurate is not acting as the other so called solid solvents such as metal alloys or even zeolites, while has a behavior more similar to that of a polar liquid solvent with a longer order range.

Acknowledgments

RCD was supported through a fellowship of the Prometeo Project issued by the Secretary of Higher Education, Science, Technology and Innovation of Ecuador (*Secretaría de Educación Superior, Ciencia, Tecnología e Innovación de la República del Ecuador*). This project was also partially supported by the Spanish Government under the project TACTICA.

References

[1] M.L. Cohen, Phys. Rev. B Condens Matter 32 (1985) 7988–7991.
[2] A.Y. Liu, M.L. Cohen, Phys. Rev. B Condens Matter 41 (1990) 10727–10734.
[3] X. Li, J. Zhang, L. Shen, Y. Ma, W. Lei, Q. Cui, G. Zou, Appl. Phys. A 94 (2008) 387–392.
[4] Y. Zhao, Z. Liu, W. Chu, L. Song, Z. Zhang, D. Yu, Y. Tian, S. Xie, L. Sun, Adv. Mater. 20 (2008) 1777–1781.
[5] R.C. Dante, J. Martín-Gil, L. Pallavidino, F. Geobaldo, J. Macromol. Sci., Part B 49 (2010) 371–382.
[6] G. Zhang, M. Zhang, X. Ye, X. Qiu, S. Lin, X. Wang, Adv. Mater. 26 (2014) 805–809.
[7] J. Zhang, J. Sun, K. Maeda, K. Domen, P. Liu, M. Antonietti, X. Fu, X. Wang, Energy Environ. Sci. 4 (2011) 675.
[8] Y. Zhang, X. Bo, A. Nsabimana, C. Luhana, G. Wang, H. Wang, M. Li, L. Guo, Biosens. Bioelectron. 53 (2014) 250–256.
[9] Y. Zhang, T. Mori, J. Ye, Sci. Adv. Mater. 4 (2012) 282–291.
[10] Y. Zhang, Z. Schnepp, J. Cao, S. Ouyang, Y. Li, J. Ye, S. Liu, Sci. Rep. 3 (2013).
[11] A. Vinu, K. Ariga, T. Mori, T. Nakanishi, S. Hishita, D. Golberg, Y. Bando, Adv. Mater. 17 (2005) 1648–1652.
[12] H. Zhao, M. Lei, X.a. Yang, J. Jian, X. Chen, J. Am. Chem. Soc. 127 (2005) 15722–15723.
[13] J.L. Zimmerman, R. Williams, V.N. Khabashesku, J.L. Margrave, Nano Lett. 1 (2001) 731–734.
[14] C. Cao, F. Huang, C. Cao, J. Li, H. Zhu, Chem. Mater. 16 (2004) 5213–5215.
[15] A. Thomas, A. Fischer, F. Goettmann, M. Antonietti, J.-O. Müller, R. Schlögl, J.M. Carlsson, J. Mater. Chem. 18 (2008) 4893.
[16] L.M. Zambov, C. Popov, N. Abedinov, M.F. Plass, W. Kulisch, T. Gotszalk, P. Grabiec, I.W. Rangelow, R. Kassing, Adv. Mater. 12 (2000) 656–660.
[17] S.P. Lee, J.G. Lee, S. Chowdhury, Sensors 8 (2008) 2662–2672.
[18] A. Du, S. Sanvito, Z. Li, D. Wang, Y. Jiao, T. Liao, Q. Sun, Y.H. Ng, Z. Zhu, R. Amal, S.C. Smith, J. Am. Chem. Soc. 134 (2012) 4393–4397.
[19] J. Tian, Q. Liu, A.M. Asiri, A.O. Al-Youbi, X. Sun, Anal. Chem. 85 (2013) 5595–5599.
[20] M. Deifallah, P.F. McMillan, F. Corà, J. Phys. Chem. C 112 (2008) 5447–5453.
[21] C. Li, X. Yang, B. Yang, Y. Yan, Y. Qian, Mater. Chem. Phys. 103 (2007) 427–432.
[22] R.C. Dante, P. Martín-Ramos, A. Correa-Guimaraes, J. Martín-Gil, Mater. Chem. Phys. 130 (2011) 1094–1102.
[23] A. Heine, K. Gloe, T. Doert, K. Gloe, Zeitschrift für anorganische und allgemeine Chemie 634 (2008) 452–456.
[24] R.C. Dante, P. Martín-Ramos, L.M. Navas-Gracia, F.M. Sánchez-Arévalo, J. Martín-Gil, J. Macromol. Sci. Part B 52 (2013) 623–631.
[25] R.C. Dante, P. Martín-Ramos, F.M. Sánchez-Arévalo, L. Huerta, M. Bizarro, L.M. Navas-Gracia, J. Martín-Gil, J. Solid State Chem. 201 (2013) 153–163.
[26] P. Chamorro-Posada, J. Vázquez-Cabo, F.M. Sánchez-Arévalo, P. Martín-Ramos, J. Martín-Gil, L.M. Navas-Gracia, R.C. Dante, J. Solid State Chem. 219 (2014) 232–241.
[27] J.L. Sessler, P.A. Gale, W.-S. Cho, Anion Receptor Chemistry, RSC Publishing, Cambridge, 2006.
[28] J.A. Zerkowski, C.T. Seto, G.M. Whitesides, J. Am. Chem. SOC. 114 (1992) 5473.
[29] A. Ranganathan, V.R. Pedireddi, C.N.R. Rao, J. Am. Chem. Soc. 121 (1999) 1752.
[30] M. Nowak, B. Kauch, P Szperlich, Rev. Sci. Instrum 80 (2009) 046107.
[31] L. Duvillaret, F. Garet, J.L. Coutaz, IEEE J. Select. Top. Quant. Electron. 2 (1996) 739–746.
[32] J.D.C. Maia, G.A.U. Carvalho, C.P. Mangueira, S.R. Santana, L.A.F. Cabral, G.B. Rocha, J. Chem. Theory Comput. 8 (2012) 3072–3081.
[33] J.J.P. Stewart, Stewart Computational Chemistry, Colorado Springs, CO, USA, 2012 ⟨http://openmopac.net⟩.
[34] B. Jürgens, E. Irran, J. Senker, P. Kroll, H. Müller, W. Schnick, J. Am. Chem. Soc. 125 (2003) 10288–10300.
[35] J.J.P. Stewart, J. Mol. Mod 13 (2007) 1173–1213.
[36] C.F. Macrae, P.R. Edgington, P. McCabe, E. Pidcock, G.P. Shields, R. Taylor, M. Towler, J. van de Streek, J. Appl. Cryst. 39 (2006) 453–457.
[37] Z.A. Fekete, E.A. Hoffmann, T. Körtvélyesi, B. Penke, Mol. Phys. 105 (19–22) (2007) 2597–2605 10 October–20 November.
[38] A.R. Allouche, J. Comput. Chem. 32 (2010) 174–182.